AIAA Aviation
13-17 June 2016, Washington, D.C.
46th AIAA Fluid Dynamics Conference

High Order Entropy Stable Discontinuous Galerkin Schemes in a Space-Time Computational Framework

Mohammad Zakerzadeh * and Georg May †
Graduate School AICES, RWTH Aachen, 52062 Aachen, Germany

In this paper we present a space-time computational framework for solution of nonlinear hyperbolic systems of conservation laws. The framework is based on a previously proposed space-time discontinuous Galerkin discretization, realized in terms of entropy variables. Building on previous stability and convergence analysis, the main aim of the present paper is to address the increased complexity of the high-order implicit space-time formulation. We propose a time-marching scheme of the tent-pitching type, maintaining the implicit nature of the solution algorithm, as well as high order temporal accuracy, while avoiding global space-time coupling of the degrees of freedom. The algorithm is introduced and numerical experiments for different linear and nonlinear test cases are presented.

I. Introduction

The class of nonlinear systems of conservation laws contains many important examples. A case in point are the Euler equations and the Navier-Stokes equations, governing inviscid and viscous compressible fluid flow, respectively. When analyzing the stability of numerical schemes for such systems, entropy stability is often the framework of choice.[3–5,7,9,15,17,18,23,24,36,37] For finite element schemes in particular, space-time formulation often facilitates establishing stability and, as the case might be, convergence. Space-time formulations of the continuous Galerkin (CG) type with streamline diffusion stabilization are classic.[26,27,34,35] An extension of these classic schemes to discontinuous Galerkin (DG) methods, which are of particular interest in the present work, is also available.[25] These schemes can be proved convergent for the case of scalar conservation laws. For systems of conservation laws various entropy stable DG schemes have been presented.[3–5,9] Recently, space-time DG Schemes of arbitrary order for hyperbolic systems of conservation laws that (under appropriate assumptions) converge at least to an entropy-measure-valued (EMV) solution have been proposed.[22,42]

In particular, our recently proposed class of DG schemes for nonlinear hyperbolic systems of conservation laws[42] uses merely a suitable entropy-stable flux,[37] as well as a nonlinear shock-capturing term, for stabilization. We have proved that our method is entropy stable and satisfies a suitable global entropy inequality. Also, we have proved that uniformly bounded solutions convergence to an entropy measure-valued solution for arbitrary (fixed) order of polynomial approximation. The schemes in[22] are similar in nature, and yield the same analytical results. The main difference is that in our formulation, no streamline diffusion is needed. Adding streamline diffusion stabilization facilitates proofs (especially) of entropy consistency and convergence, but does not really reflect the way DG schemes are most often implemented for compressible flow simulation.[6,8,20,21,40]

While a space-time formulation is very convenient from an analysis point of view, a naive implementation as a steady problem on a $d+1$-dimensional space-time mesh (where $d = 1, 2, 3$ is the spatial dimension), may be computationally costly. This is potentially true even if one takes advantage of time-causality by pure upwinding in time on space-time slabs. Even in this case, one still solves a nonlinear system globally coupled in space (on each space-time slab) with additional degrees of freedom for the resolution on the time variable. At the very least the storage requirements may be dramatic. A potentially attractive alternative are the so-called *tent pitcher* algorithms[14] which take advantage not only of time-causality but also of finite speed of propagation in hyperbolic problems in a constructive way. Tent pitching algorithms generate advancing front

*Graduate student.
†Associate professor.

time dependent local meshes, such that one can solve the problem locally element by element, or in practice on a very small local patch of elements. This is possible if new local elements are constructed in such a manner that all new boundary faces of the patch of elements are *causal* faces,[30] i.e. faces with no information coming into the cell. The faces which are not causal are called *coupled*. There are numerous examples of tent-pitching methods.[1,14,29,39,41] In this paper we apply the tent pitcher algorithm[39] for simplex elements to construct a computationally efficient framework of the method presented in Zakerzadeh and May.[42]

The outline of this paper is as follows: The governing equations and relevant solution concepts are recalled in §II. The space-time DG framework is introduced in §III. This section also includes the general form of the numerical diffusion and shock capturing operators. For more details on these we refer to §IV and Reference 42. Also in this section, the fully discrete entropy inequality of the solution and its BV-estimate are presented as well as the L_2 stability result. Furthermore, in §IV we provide some numerical examples to show the applicability and efficiency of the method.

II. Governing equations

The general form of a nonlinear $m\times m$-system of conservation laws in several space dimensions is

$$\boldsymbol{u}_t + \sum_{k=1}^{d} \boldsymbol{f}^k(\boldsymbol{u})_{x_k} = 0, \tag{1}$$

where the unknowns $\boldsymbol{u} = \boldsymbol{u}(x,t)\colon \mathbb{R}^d \times [0,\infty) \to \mathbb{R}^m$ are the *conserved variables* and $\boldsymbol{f}^k\colon \mathbb{R}^m \to \mathbb{R}^m$, $k = 1,\dots,d$ are (nonlinear) smooth *flux functions* with $d = 1,2,3$.

The conservation laws have to be augmented with initial conditions, as well as suitable boundary conditions. In this introductory section, we assume that (1) is solved as a Cauchy problem on $\mathbb{R}^d$, with initial conditions $\boldsymbol{u}_0(x)$, assumed to have compact support, to avoid technicalities arising from boundary conditions. (Finite speed of propagation in hyperbolic problems then implies that the solution $\boldsymbol{u}(x,t)$ has compact support for any finite time t and vanishes for $|x|$ large.)

For the numerical experiments considered, we solve one-dimensional (d=1) model equations, the shallow-water equations, as well as the Euler equations of compressible gas dynamics. The specific equations are given in §IV.

A. Weak and measure-valued solution

It is well-known that equations of the type (1) can produce discontinuities in finite time; hence the solution cannot be interpreted in the classical sense. This motivates one to introduce the concept of *weak solution* which is defined as a bounded function $\boldsymbol{u}$ that satisfies (1) in distributional sense, i.e.

$$\int_0^\infty \int_{\mathbb{R}^d} \Big(\langle \boldsymbol{u}, \boldsymbol{\varphi}_t \rangle + \sum_{k=1}^{d} \langle \boldsymbol{f}^k(\boldsymbol{u}), \boldsymbol{\varphi}_{x_k} \rangle \Big) \,\mathrm{d}x\,\mathrm{d}t + \int_{\mathbb{R}^d} \langle \boldsymbol{\varphi}(x,0), \boldsymbol{u}_0(x) \rangle \,\mathrm{d}x = 0, \tag{2}$$

for all functions $\boldsymbol{\varphi} \in (\mathcal{C}_c^\infty(\mathbb{R}^d \times [0,\infty)))^m$. Here the notation $\langle \boldsymbol{u}, \boldsymbol{w} \rangle$ denotes the inner product between vectors $\boldsymbol{u}$ and $\boldsymbol{v}$ in state space $\mathbb{R}^m$. Also we will use the notation $\boldsymbol{a}\cdot\boldsymbol{b}$ as the notation for the inner product of vectors $\boldsymbol{a}$ and $\boldsymbol{b}$ in physical space $\mathbb{R}^d$.

Weak solutions are not necessarily unique nor physical; an *entropy inequality condition* is used to single out the physically admissible solutions. Assume that there exists a pair of functions (U,F), $U\colon \mathbb{R}^m \to \mathbb{R}$ and $\boldsymbol{F} = (F^1,\dots,F^d)^T\colon \mathbb{R}^m \to \mathbb{R}^d$ such that U is convex and $\partial_{\boldsymbol{u}} F^k(\boldsymbol{u}) = \partial_{\boldsymbol{u}} U(\boldsymbol{u}) \partial_{\boldsymbol{u}} \boldsymbol{f}^k(\boldsymbol{u})$ for all $1 \le k \le d$. Then, U and $\boldsymbol{F}$ are called *entropy function* and *entropy flux*, respectively, and the admissibility for weak solutions depends on the consistency with the *entropy inequality*

$$U(\boldsymbol{u})_t + \sum_{k=1}^{d} F^k(\boldsymbol{u})_{x_k} \le 0, \tag{3}$$

in the distributional sense for all entropy-entropy flux pairs corresponding to the system (1). Applying this admissibility condition, one can select a unique solution for a scalar conservation law, termed the *entropy weak solution* (see Kružkov[28]). This is basically the result of 'richness' of the family of entropy pairs; while

the lack of enough entropies for general systems is the main reason why the well-posedness of the weak solution is still an open problem for general systems.

By defining *entropy variables* as $\boldsymbol{v} = (U_{\boldsymbol{u}})^T$ one can recast (1) in symmetric form as

$$\boldsymbol{u}_{\boldsymbol{v}}\boldsymbol{v}_t + \sum_{k=1}^{d} \boldsymbol{f}_{\boldsymbol{v}}^k \boldsymbol{v}_{x_k} = 0, \tag{4}$$

such that the matrix $\boldsymbol{u}_{\boldsymbol{v}}$ is symmetric positive definite and the matrices $\boldsymbol{f}_{\boldsymbol{v}}^k$ are symmetric. This formulation simplifies the analysis of *entropy stability*, for both the infinite-dimensional weak solution and its finite-dimensional numerical approximation counterpart, as well as the implementation of entropy-stable numerical schemes. Integrating (3) for a solution with compact support leads to the following *global entropy inequality*

$$\frac{\mathrm{d}}{\mathrm{d}t}\int_{\mathbb{R}^d} U(\boldsymbol{u})\,\mathrm{d}x \leq 0 \Longrightarrow \int_{\mathbb{R}^d} U(\boldsymbol{u}(x,T))\,\mathrm{d}x \leq \int_{\mathbb{R}^d} U(\boldsymbol{u}(x,0))\,\mathrm{d}x. \tag{5}$$

This property can be viewed as an extension of L_2 stability for systems of conservation laws and is desirable to be retained for the approximate solution $\boldsymbol{u}^h$ as well. This is the motivation behind *entropy stable schemes*, which were originally introduced by Tadmor.[36]

Satisfying entropy stability, however, is not at all sufficient to conclude any sort of convergence for a numerical scheme in the general case. In particular, for arbitrary-order DG schemes, results are not easy to come by. In fact, trying to obtain some sort of convergence for systems of conservation laws leads to an even weaker notion of solution, the so-called *entropy measure-valued* (EMV) solutions. These types of solutions, introduced by DiPerna,[12] are more general than weak solutions. The solution is essentially viewed as a probability measure which satisfies the governing equations are satisfied in a moment sense (and still in the sense of distributions.) This permits a meaningful convergence theory for numerical schemes approximating (1). In the present paper, however, we shall focus on more practical issues. We give a brief summary of the stability properties of our scheme in §III.D, but we shall not discuss convergence here. For a brief review of measure-valued solutions and convergence results for numerical approximation we refer to Zakerzadeh and May,[42] or Hiltebrand and Mishra.[22]

III. Shock-capturing DG formulation

Here, we introduce the shock capturing discontinuous Galerkin (SC-DG) method for nonlinear systems of conservation laws (1). A space-time framework, similar to that used in[22,26,27,34,35,42] is proposed for discretization of the problem. First we introduce the space-time triangulation and present the DG approximation, including the structure of the shock capturing term. Then we outline the tent pitcher method and how it exploits the causality to solve a hyperbolic problem in an element-by-element (or in fact tent-by-tent) manner.

A. Space-time triangulation

Adopting the compact support assumption for the solution in a finite time interval $[0,T]$, we consider the space domain $\Omega \subset \mathbb{R}^d$ such that $\operatorname{supp} \boldsymbol{u}(\cdot,t) \subset \Omega$ at each time $t \in [0,T]$. In order to discretize (1), let $0 = t_0 < t_1 < ... < t_N = T$ be a sequence representing discrete time steps, and let $I_n = [t_n, t_{n+1})$ be the corresponding time intervals. We also denote the space-time domain by $\Omega \times [0,T]$.

Let consider a subdivision $\mathcal{T}_n = \{\kappa\}$ of S_n into disjoint convex finite elements on each space-time slab, $S_n = \Omega \times I_n$, with interface members $\kappa_j \cap \kappa_j,\ i \neq j$ of measure $d'-1$. Here, d' denotes the dimension of the space-time which is equal to $d+1$.

Without loss of generality, let us assume that

$$h = \sup_{\kappa,n} h_\kappa < \infty, \qquad \kappa \in \mathcal{T}_n, n \in \{0,\ldots,N-1\}, \tag{6}$$

where h_κ is the exterior diameter of a space-time cell κ. The interior diameter of an element (the diameter of the inscribed circle) is denoted by ρ_κ. We assume the following quasi-uniformity condition

$$\frac{h}{\rho_\kappa} \leq \sigma, \qquad \forall \kappa \in \mathcal{T}_n, \tag{7}$$

with $\sigma > 0$ independent of h. The perimeter of κ is defined by $p_\kappa = \Sigma_{e\in\partial\kappa}|e|$, where $|e|$ is the d-measure of the face. The uniformity assumption (7) implies that[10]

$$\frac{1}{\mu} \leq \frac{p_\kappa h_\kappa}{|\kappa|} \leq \mu, \qquad \forall \kappa \in \mathcal{T}_n, \tag{8}$$

for some $\mu > 0$ independent of h. Typically, κ might be a tetrahedron or a prism defined as $K \times I_n$, where K corresponds to spatial triangulation on $\mathbb{R}^d$. In Ref.42 we presented the formulation for prism elements merely to avoid more complicated notation for simplices. Here, due to the tent pitcher time marching we are presenting, it is required to have simplex space-time elements, and we need to modify the formulation of Ref. 42 somewhat. Moreover, note that in the tent pitcher approach there is no longer the need to use time slabs and the computation can be done tent-by-tent until the final time T is reached. Also, as e.g. in Ref. 19, time slabs can be used safely with tent pitching algorithms. (In this case there will simply be no global coupling in each time interval.) For convenience, we will stick to the slab notation. If no time slabs are used, one can simply set $n = 1$, $t_n = T$ and $S_n = \Omega \times [0, T]$ to be consistent.

B. Variational formulation

The finite dimensional space for the approximate solution is defined as

$$\mathcal{V}_n^q = \{\boldsymbol{w} \in (L_2(S_n))^m : \boldsymbol{w}|_\kappa \in (\mathbb{P}_q(\kappa))^m, \forall \kappa \in \mathcal{T}_n\}, \qquad n = 0, \ldots, N-1, \tag{9}$$

where $\mathbb{P}_q(\kappa)$ is the space of polynomials of at most degree q for a domain $\kappa \subset \mathbb{R}^{d'}$. We also denote $\mathcal{V}^q = \prod_{n=0}^{N-1} \mathcal{V}_n^q$ as the approximation space in global space-time domain. The approximating functions are considered discontinuous both in space and time.

The proposed shock capturing discontinuous Galerkin method has the following quasi-linear (nonlinear in first argument and linear in the second one) variational form in terms of entropy variables: Find $\boldsymbol{v}^h \in \mathcal{V}^q$ such that for each $n = 0, \ldots, N-1$, $\boldsymbol{v}^h|_{S_n} \in \mathcal{V}_n^q$ satisfies,

$$\mathcal{B}(\boldsymbol{v}^h, \boldsymbol{w}^h) = \mathcal{B}_{DG}(\boldsymbol{v}^h, \boldsymbol{w}^h) + \mathcal{B}_{SC}(\boldsymbol{v}^h, \boldsymbol{w}^h) = 0, \qquad \forall \boldsymbol{w}^h \in \mathcal{V}^q. \tag{10}$$

Note that we realize the functions in terms of entropy variables $\boldsymbol{v}^h$ which are the basic unknowns and the dependent conservative variables are derived via mapping $\boldsymbol{u}(\boldsymbol{v}^h)$. In our notation, this mapping is sometimes omitted, e.g., $\boldsymbol{f}(\boldsymbol{v}^h)$ is written rather than $\boldsymbol{f}(\boldsymbol{u}(\boldsymbol{v}^h))$.

Using the test function $\boldsymbol{w}^h \in \mathcal{V}^q$ to penalize the interior residual of the cell and jump of the fluxes which leads to

$$\mathcal{B}_{DG}(\boldsymbol{v}^h, \boldsymbol{w}^h) = -\sum_{\kappa,n} \int_\kappa \langle \nabla \cdot \tilde{\boldsymbol{f}}, \boldsymbol{w}^h \rangle \, \mathrm{d}\bar{x} + \sum_{\kappa,n} \int_{\partial\kappa} \langle \hat{\boldsymbol{f}}(\boldsymbol{v}^h) - \tilde{\boldsymbol{f}}(\boldsymbol{v}_-^h) \cdot \boldsymbol{n}, \boldsymbol{w}_-^h \rangle \, \mathrm{d}s, \tag{11}$$

where $\tilde{\boldsymbol{f}} = (\boldsymbol{u}, \boldsymbol{f}(\boldsymbol{u}))$ is the space-time flux, and at every point $\bar{x} \in \mathbb{R}^{d'}$ on $\partial\kappa$ we define the notation $\boldsymbol{w}_\pm^h(\bar{x}) = \lim_{\epsilon\to 0} \boldsymbol{w}^h(\bar{x} \pm \epsilon \boldsymbol{n})$ for values on element interfaces. Here $\boldsymbol{n} = (n_t, n_{x_1}, \cdots, n_{x_d})$ is the outward pointing normal on $\partial\kappa$ at $\bar{x}$. Also we assume that the initial data $\boldsymbol{v}_{0,-}^h = \boldsymbol{v}^h(x, 0_-)$ is obtained from a suitable projection of the initial data $\boldsymbol{v}_0(x) = \boldsymbol{v}(\boldsymbol{u}_0(x))$.

Here, $\hat{\boldsymbol{f}}(\boldsymbol{v}^h) = \hat{\boldsymbol{f}}(\boldsymbol{v}_{\kappa,-}^h, \boldsymbol{v}_{\kappa,+}^h; \boldsymbol{n})$ denotes the space-time numerical flux function, a vector-valued function of two interface states $\boldsymbol{v}_\pm^h$ and the interface normal $\boldsymbol{n}$, which is considered to be conservative and consistent with $\tilde{\boldsymbol{f}}$. In order that the variational problem is independently solvable at each time slab level (and also at tent level), on the interfaces where $(\pm 1, 0, \cdots, 0)$ we assume that the numerical flux reduces to the pure upwinding in time. Also the spatial part of this numerical flux is supposed to be entropy stable, i.e. we consider it in the viscosity form as

$$\hat{\boldsymbol{f}}(\boldsymbol{v}^h)_{\text{spatial}} = \hat{\boldsymbol{f}}(\boldsymbol{v}_-^h, \boldsymbol{v}_+^h; (0, n_{x_1}, \cdots, n_{x_d})) = \boldsymbol{f}^\star(\boldsymbol{v}^h) - \frac{1}{2} D(\boldsymbol{v}^h)\big(\boldsymbol{v}_+^h - \boldsymbol{v}_-^h\big), \tag{12}$$

where $\boldsymbol{f}^\star(\boldsymbol{v}^h) = \boldsymbol{f}^*(\boldsymbol{v}_-^h, \boldsymbol{v}_+^h; \boldsymbol{n})$ denotes the *entropy conservative flux* and D is the numerical diffusion required to obtain entropy stability, which is a set to a symmetric and uniformly positive definite matrix. Two interesting choices for diffusion matrix D are Roe and Rusanov diffusion. We refer to[18,24,37] for more details on the diffusion matrix and properties of the entropy stable fluxes as well as explicit forms of such fluxes for shallow water and Euler equations.

C. Shock capturing operator

In order to stabilize the scheme in the presence of discontinuities we need to add a form of artificial viscosity. We expect this operator to add a significant stabilization effect close to discontinuities, while only a little viscosity is added in smooth regions. In this formulation, the residual of the finite element solution is used as a sensor for presence of discontinuities. Let introduce the shock capturing operator as

$$\mathcal{B}_{SC}(\boldsymbol{v}^h, \boldsymbol{w}^h) = \sum_{\kappa,n} \int_\kappa \varepsilon_\kappa \Big(\langle \boldsymbol{w}_t^h, \tilde{\boldsymbol{u}}_{\boldsymbol{v}} \boldsymbol{v}_t^h \rangle + \sum_{k=1}^{d} \langle \boldsymbol{w}_{x_k}, \tilde{\boldsymbol{u}}_{\boldsymbol{v}} \boldsymbol{v}_{x_k} \rangle \Big) \, \mathrm{d}\bar{x}, \tag{13}$$

where the viscosity ε_κ is defined as

$$\varepsilon_\kappa = \frac{h^\alpha C_1^{SC} \overline{\mathrm{Res}}_\kappa}{\overline{\nabla \boldsymbol{v}}_\kappa + h^\theta}. \tag{14}$$

Here, $\overline{\mathrm{Res}}_\kappa^2$ and $\overline{\nabla \boldsymbol{v}}_\kappa$ are weighted residual and gradient of the solution $\boldsymbol{v}^h$, respectively and defined as the following

$$\overline{\nabla \boldsymbol{v}}_\kappa^2 = \int_\kappa \langle \boldsymbol{v}_t^h, \tilde{\boldsymbol{u}}_{\boldsymbol{v}} \boldsymbol{v}_t^h \rangle + \sum_{k=1}^{d} \langle \boldsymbol{v}_{x_k}^h, \tilde{\boldsymbol{u}}_{\boldsymbol{v}} \boldsymbol{v}_{x_k}^h \rangle \, \mathrm{d}\bar{x}, \tag{15}$$

$$\overline{\mathrm{Res}}_\kappa^2 = \int_\kappa \langle \mathrm{Res}, \boldsymbol{v}_{\boldsymbol{u}}(\boldsymbol{v}^h(x,t)) \mathrm{Res} \rangle \, \mathrm{d}\bar{x}. \tag{16}$$

Here $\tilde{\boldsymbol{u}}_{\boldsymbol{v}}$ denotes $\boldsymbol{u}_{\boldsymbol{v}}(\tilde{\boldsymbol{v}}_\kappa)$ and $\tilde{\boldsymbol{v}}_\kappa$ is the cell average defined as

$$\tilde{\boldsymbol{v}}_\kappa = \frac{1}{|\kappa|} \int_\kappa \boldsymbol{v}^h(x,t) \, \mathrm{d}\bar{x}. \tag{17}$$

Moreover, the local residual is defined as $\mathrm{Res} = \boldsymbol{u}(\boldsymbol{v}^h)_t + \sum_{k=1}^{d} \boldsymbol{f}^k(\boldsymbol{v}^h)_{x_k}$.

In (13), C^{SC} is a positive constants and h^θ is added as the regularization parameter with parameter $\theta \geq \frac{d'-\alpha}{2}$. Also the viscosity strength parameter $\alpha \in (0,2)$. The rationale behind the specific form of the shock-capturing operator, and the choices for θ and α are discussed in our original publication of the scheme.[42] In essence, these choices are such that we can guarantee the convergence of the approximate solution to an EMV solution.

D. Energy analysis

We have previously proved that the approximate solution of (1), coming from the proposed scheme (10), satisfies the global entropy inequality in the fully discrete sense.[42] Then, by adopting some additional assumptions, a weak BV-estimate was also proved. Here we just present the results and refer to Ref. 42 for more details on the proofs.

The entropy stability result is given as the following theorem:

Theorem 1 (Theorem 4.1 of Ref. 42)**.** *Consider the system of conservation laws* (1)*, equipped with strictly convex entropy function U and corresponding entropy flux functions $F^k, k = 1, \ldots, d$. Furthermore, assume that the exact and approximate solutions have compact support inside the spatial domain Ω. Then, the shock capturing discontinuous Galerkin scheme* (10) *approximating* (1) *has the following properties:*

(i) The scheme (10) *is conservative in the following sense: If $\boldsymbol{u}^h = \boldsymbol{u}(\boldsymbol{v}^h)$ is the approximate solution, then*

$$\int_\Omega \boldsymbol{u}(\boldsymbol{v}^h(x, t_-^N)) \, \mathrm{d}x = \int_\Omega \boldsymbol{u}(\boldsymbol{v}^h(x, t_-^0)) \, \mathrm{d}x. \tag{18}$$

(ii) The scheme (10) *is entropy stable i.e., the approximate solution $\boldsymbol{u}^h$ admits the following fully discrete global entropy bounds,*

$$\int_\Omega U(\boldsymbol{u}^*(t_-^0)) \, \mathrm{d}x \leq \int_\Omega U(\boldsymbol{u}(\boldsymbol{v}^h(x, t_-^N))) \, \mathrm{d}x \leq \int_\Omega U(\boldsymbol{u}(\boldsymbol{v}^h(x, t_-^0))) \, \mathrm{d}x, \tag{19}$$

where $\boldsymbol{u}^*(t_-^0)$ is called the minimum total entropy state of the projected initial data and is defined as

$$\boldsymbol{u}^*(t_-^0) = \frac{1}{|\Omega|} \int_\Omega \boldsymbol{u}(\boldsymbol{v}^h(x, t_-^0)) \, \mathrm{d}x. \tag{20}$$

Now let assume that there exist some constants independent of $\boldsymbol{v}^h$ such that $\forall \boldsymbol{w} \neq 0$

$$0 < c\langle \boldsymbol{w}, \boldsymbol{w}\rangle \leq \langle \boldsymbol{w}, \boldsymbol{u}_{\boldsymbol{v}}(\boldsymbol{v}^h(x,t))\boldsymbol{w}\rangle \leq C\langle \boldsymbol{w}, \boldsymbol{w}\rangle. \tag{21}$$

as well as a uniform spectral upper bound for $\boldsymbol{f}_{\boldsymbol{v}}$, i.e.

$$\langle \boldsymbol{w}, \boldsymbol{f}_{\boldsymbol{v}}\boldsymbol{w}\rangle \leq C\langle \boldsymbol{w}, \boldsymbol{w}\rangle, \qquad \forall \boldsymbol{w} \neq 0, \tag{22}$$

where C is uniform and independent of $\boldsymbol{w}$. Then, we can prove the following weak BV-estimate for the approximation solution of the scheme (10):

Corollary 1 (Corollary 4.4. of Ref. 42)**.** *Let the assumptions of Theorem 1 as well as* (21)*,* (22) *and the uniform positive definiteness of D hold. Then the approximate solution* $\boldsymbol{v}^h$ *satisfies the following weak BV-estimate:*

$$\sum_{\kappa,n}\int_{\kappa} |\boldsymbol{v}^h_+ - \boldsymbol{v}^h_-|^2 \,\mathrm{d}s + h^{\alpha}\sum_{\kappa,n}\overline{\mathrm{Res}}_{\kappa}\|\nabla \boldsymbol{v}^h\|_{L_2(\kappa)} \leq C, \tag{23}$$

where C *is a positive constant dependent on the initial condition* $\boldsymbol{u}_0$*.*

Another interesting result one can look at, is the L_2 stability of the solution. This result is trivially given for scalar case or symmetric systems by the proven entropy stability with $U(\boldsymbol{u}) = \frac{1}{2}|\boldsymbol{u}|^2$ as the provided entropy function. It is desired to extract some sort of familiar L_2 stability for general nonlinear cases. We have:

Corollary 2 (cf. Ref. 5)**.** *Under the assumption* (21) *the following* L_2 *stability is readily obtained*

$$\|\boldsymbol{u}(\boldsymbol{v}^h(x,t^N_-)) - \boldsymbol{u}^*(t^0_-)\|_{L_2(\Omega)} \leq \sqrt{\frac{C}{c}}\,\|\boldsymbol{u}(\boldsymbol{v}^h(x,t^0_-)) - \boldsymbol{u}^*(t^0_-)\|_{L_2(\Omega)}, \tag{24}$$

where $\boldsymbol{u}^*$ *is defined as* (20) *and* c, C *are same constants as in* (21)*.*

E. Tent-pitcher algorithm

As mentioned in §I, the goal of a tent-pitcher algorithm at each step is to make a mesh such that it has only causal boundary faces and is therefore solvable independently. In general, it is not practical to generate an element-wise mesh with this property. However, it is possible to construct a *tent* made of M elements such that it has only causal new boundary faces, while the elements within each tent are coupled to each other and thus need to be solved simultaneously. One can prove[39] that if the maximum number of neighbours in the subdomain d-dimensional mesh is M, the the algorithm guarantees that we do not need to construct tents containing more than M elements as time evolves. Since M is independent of the total number of elements, N, this property ensures that the workload of solving each tent remains N-independent, and the total complexity for fixed q is $\mathcal{O}(N)$.

For details we refer to numerous references on tent pitching[1, 1, 29, 39] and the references cited therein. In order to give an overview of the algorithm, let us start by considering a triangulation $\mathcal{T}_h$ of the spatial domain Ω, into some disjoint convex d-dimensional elements. We denote the set of vertices of this triangulation as $\{p_i\}_{i=1,\cdots,\mathcal{N}_\mathcal{T}}$ where $\mathcal{N}_\mathcal{T}$ is the total number of vertices of $\mathcal{T}_h$. Let us define the *advancing front* function as

$$\tau : \Omega \to \mathbb{R}_+, \qquad \tau \in \mathcal{Q}^1(\mathcal{T}_h), \tau_i = \tau(p_i), \tag{25}$$

where by $\mathcal{Q}^1(\mathcal{T}_h)$, we mean continuous linear polynomials defined on $\mathcal{T}_h$. The graph of τ represents the evolution front of the solution, i.e. for any $x \in \Omega$, $\boldsymbol{u}(x,t)$ is known for $0 \leq t \leq \tau(x)$.

The general structure of the algorithm is to find an *adequate* vertex p_i for the base of the tent and an *admissible* update of τ_i, denoted by τ_i^{new}. Then it generates a tent made of τ_i^{new} and all $\tau(p_j)$; where $p_{j,j\neq i}$ are the neighbouring vertices connected to p_i by a single edge, as well as the old value of advancing front at p_i, denoted by τ_i^{old}.

Note that we call an update admissible when the corresponding tent of such an update has only causal external faces. Moreover, choosing of an adequate base p_i can be done using various criteria,[39] which influence the quality of the final mesh. Here we just mention the main criterion that we do not allow the base point to be located on the *peak* or *slope* on the old advancing front graph; i.e. the admissible p_i must be the local minimum of the neighbouring region.

In particular we apply the following steps:

(i) At the initial time we set $\tau \equiv 0$ for all $x \in \Omega$ and calculate the maximum initial speed of data propagation at each element.

(ii) We choose an adequate base node, p_i and construct a tent by updating the τ value of its apex as $\tau_i^{\text{new}} = \tau_i^{\text{old}} + \delta\tau_i$ alongside the time axis and connecting it to p_i and all its neighbouring vertices $p_{j,j\neq i}$.

(iii) The update value $\delta\tau_i$ is calculated based on the maximum wave speed that reaches the tent. While in linear problems this can be precomputed and it would be local, in nonlinear problems we need to search globally. For this reason we used the global maximum wave speed on all (integration) points residing on $(\tau(x), x)$ for all $x \in \Omega$ in space-time domain. Another approach is efficiently based on a binary search and is explained in detail in Reference 38.

(iv) The resulting tent composed of at most M coupled elements which are solved simultaneously. Then we update the τ function and repeat steps (ii)-(iv) till the final time t_n (which may be simply $t_n = T$ if no time slabs are used.) is achieved, i.e. $\tau_i = t_n$ for all i.

IV. Numerical results

In this section we present some numerical experiments in one space dimension to validate the code and assess the efficiency of the scheme. Extension of the code to higher spatial dimensions is planned for future work. First, in section A, we solve a linear system of the one dimensional wave equation to show that the order of convergence is optimal. For the proof of convergence to the unique entropy solution in this case we refer to Hiltebrand and Mishra.[22] As examples of more general systems, we present in section B a numerical solution of the dam break test case for the shallow water equations, as well as solutions of the one dimensional Euler equations in section C. As test cases of Euler equations we present results for the Sod and Lax shock tube, the 123 problem,[13] as well as the Shu-Osher entropy wave interaction.[33]

The Netgen/Ngsolve library[32] has been used for geometry handling and mesh generation as well as quadrature rules and the evaluation of basis functions. The nonlinear system obtained from the implicit space-time scheme is solved using a damped Newton method utilizing the ILU preconditioned GMRES available through the PETSc library.[2]

There are some free parameters in the scheme which need to be selected, including C_{SC}, α and θ. Unless otherwise mentioned explicitly we set them as $C_{SC} = 1$ and $\theta = 0.5$. The value of α is set to 1.5 for the case of wave equation and 1.1 for the rest to be more diffusive. These settings give us acceptable result in most cases.

A. Wave equations

The wave equation system in one dimension can be written as the following form

$$h_t + cu_x = 0, \tag{26}$$

$$u_t + ch_x = 0, \tag{27}$$

where c is some constant value. In this case the system is linear and symmetric in its original form and by choosing the entropy function as $U(\boldsymbol{u}) = \frac{1}{2}(h^2 + u^2)$ the entropy variables are the same as the conservative variables.

Hence, the entropy conservative flux would be the simple average of the flux values at the edge and the diffusion operator is set to Rusanov type. In our numerical test cases the boundary conditions are set to Dirichlet, the wave speed to $c = 1$ and the final time to $T = 0.5$. Also the calculation domain is considered as $[-1, 1]$. We use the following initial settings:

$$h(x, 0) = \sin(2\pi x), \qquad u(x, 0) = \sin(2\pi x)/3, \tag{28}$$

and solve for polynomial degrees $q = 0, 1, 2, 3$. The results are presented in Table 1. One can observe that adding the shock capturing term does not affect the accuracy of the scheme in terms of rate-of-convergence and asymptotically, we get the optimal order $q + 1$ in convergence of the error in L_1 norm. In general with refining the mesh, the order of convergence will be the order of consistency of the scheme, and the error levels are not significantly compromised by the SC term. The only exception is in the case $q = 3$ that we saw the reduced order of convergence in the last refinement which might come from the round off errors.

Table 1: Smooth wave problem

		$q=0$		$q=1$		$q=2$		$q=3$	
h	Elements	$\|e\|_{L_1}$	order	$\|e\|_{L_1}$	order	$\|e\|_{L_1}$	order	$\|e\|_{L_1}$	order
0.0025	300100	3.55e-2	0.959	2.85e-4	1.803	9.35e-7	2.888	7.82e-9	2.656
0.005	74900	6.91e-2	0.925	9.96e-4	1.702	6.94e-6	2.869	4.94e-8	3.876
0.01	18810	1.31e-1	0.861	3.23e-3	1.574	5.04e-5	2.827	7.19e-7	3.894
0.02	4700	2.38e-1	0.763	9.62e-3	0.854	3.58e-4	2.961	1.07e-5	4.427
0.04	1222	3.98e-1		1.71e-2		2.63e-3		2.11e-4	

Regarding the efficiency in terms of runtime using tent pitcher method, we solve the same test case by our previous version of the code,[42] which all degrees of freedom are coupled at each time slab, and the tent pitcher version looks considerably more efficient. For example running the case $q = 3$ with $h = 0.005$ (which leads to 86356 space-time elements in the old version) leads to a nearly two-fold increase in efficiency (measured in run-time.)

B. Shallow water equations

The shallow water equations which describe the disturbance propagation in incompressible fluids under the influence of gravity can be written as

$$h_t + (hu)_x = 0, \tag{29}$$

$$(hu)_t + (hu^2 + \frac{1}{2}gh^2)_x = 0, \tag{30}$$

where h and u are the depth and the velocity of the water, respectively and $g = 1$ is the gravity acceleration. The entropy function in this case is defined as the total energy $U = \frac{1}{2}\left(hu^2 + gh^2\right)$. Hence, the corresponding entropy variables and entropy conservative flux can be set as in Fjordholm et al.[18] Also we choose Rusanov type for the diffusion operator of the entropy stable flux.

Moreover, we set the initial condition for *dam break* problem as follows

$$(h, u)|_{t=0} = \begin{cases} (3, 0), & x < 0, \\ (1, 0), & x > 0. \end{cases} \tag{31}$$

We take the computational domain as $[-1, 1]$, with Dirichlet boundary condition, and the final time is set to $T = 0.2$. In Figure 1, we present the result with $q = 0, 1, 2$ versus the exact solution calculated by the SWASHES code.[11]

The result and their comparison with the exact solution shows a good control of the shock with acceptable overshoot, and the shock is quite sharp.

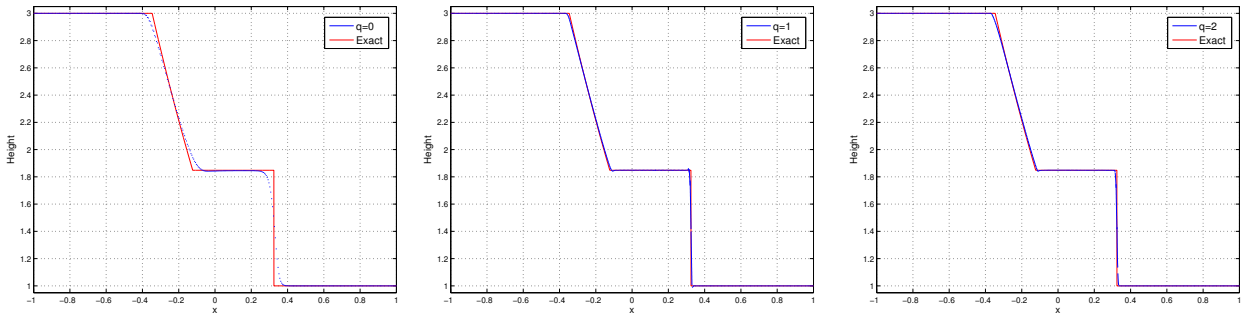

(a) $q = 0$ (b) $q = 1$ (c) $q = 1$

Figure 1: Comparison of the solution of different polynomial order DG versus exact solution, Dam break problem, height is plotted at time $t = 0.2$ on a spatial mesh of 400 elements

C. Euler equations for polytropic gas

The one-dimensional Euler equations can be written as

$$\rho_t + (\rho u)_x = 0, \tag{32}$$

$$(\rho u)_t + (\rho u^2 + p)_x = 0, \tag{33}$$

$$E_t + (u(E+p))_x = 0, \tag{34}$$

where ρ, u and E correspond to density, velocity and total energy of the gas, respectively. Here p is the pressure of the gas and is defined as $p = (\gamma - 1)(E - \frac{1}{2}\rho u^2)$, where γ is the adiabatic exponent which is set to 1.4 in all experiments here.

Following Ismail and Roe,[24] the entropy function is defined as

$$U(\boldsymbol{u}) = -\frac{\rho s}{\gamma - 1}, \tag{35}$$

where s is the specific entropy defined as $s = \ln p - \gamma \ln \rho$. The corresponding definition of entropy variables and entropy conservative flux $\boldsymbol{f}^*$, as well as that of the diffusion operator is defined according to Reference 24. We consider four types of Riemann problems for our numerical test in the domain $[-1, 1]$. The boundary conditions are set to Dirichlet type with the following initial conditions

$$(\rho, u, p)_{t=0} = \begin{cases} (\rho_L, u_L, p_L) & x < 0, \\ (\rho_R, u_R, p_R) & x \geq 0, \end{cases} \tag{36}$$

which we define as the right and left states for different cases that we present in the following sections. The exact solution is computable for all cases except the Shu-Osher test case, for which the reference solution is computed by the Compac code.[16] The type of numerical diffusion in the entropy flux is set to Roe's diffusion.[24]

1. *Sod shock tube*

Here the initial condition is in the form (36) with the values

$$(\rho_L, u_L, p_L) = (1, 0, 1), \qquad (\rho_R, u_R, p_R) = (0.125, 0, 0.1). \tag{37}$$

The results are presented in Figure 2. We observe that the shock capturing mechanism acts effectively near the shock wave and the contact discontinuity. Our solution compares well to the results by Hiltebrand and Mishra,[22] who use additional pressure scaling, as well as streamline diffusion stabilization. Moreover while increasing the polynomial degree from $q = 0$ to $q = 1$ improves the solution quality significantly the quadratic polynomial solution is quite similar to linear one, and only improves the overshooting in shock wave.

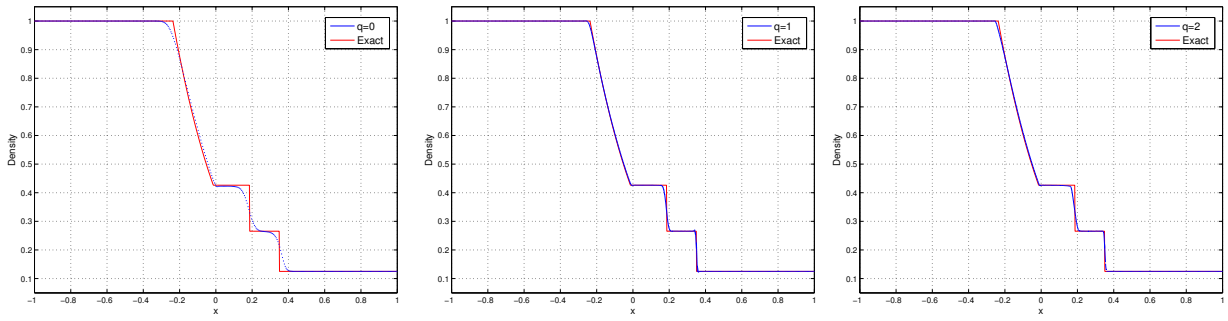

(a) $q = 0$ (b) $q = 1$ (c) $q = 2$

Figure 2: Comparison of the solution of different polynomial order DG versus exact solution, Sod shock tube problem, density is plotted at time $t = 0.2$ on a spatial mesh of 400 elements.

Also in this case, a comparison with the old scheme in terms of runtime shows that the tent pitcher method outperform the old version; e.g. the case $q = 2$ with approximately same number of elements takes $272s$ using the previous version, compared to only $20s$ using the tent pitcher.

2. *Lax shock tube*

The Lax shock tube problem is more demanding of the robustness of the scheme than the Sod problem, due to stronger shock waves. Here the initial condition is in the form (36) with values

$$(\rho_L, u_L, p_L) = (0.445, 0.698, 3.528), \qquad (\rho_R, u_R, p_R) = (0.5, 0, 0.571). \tag{38}$$

Moreover we set the final time as $T = 0.2$. Again, comparing the result in Figure 3 with Hiltebrand and Mishra[22] shows that the shock capturing mechanism is effective in alleviating the oscillations. The general behaviour here looks the same as for the Sod case but with larger overshoot in the $q = 1$ case due to the stronger shock.

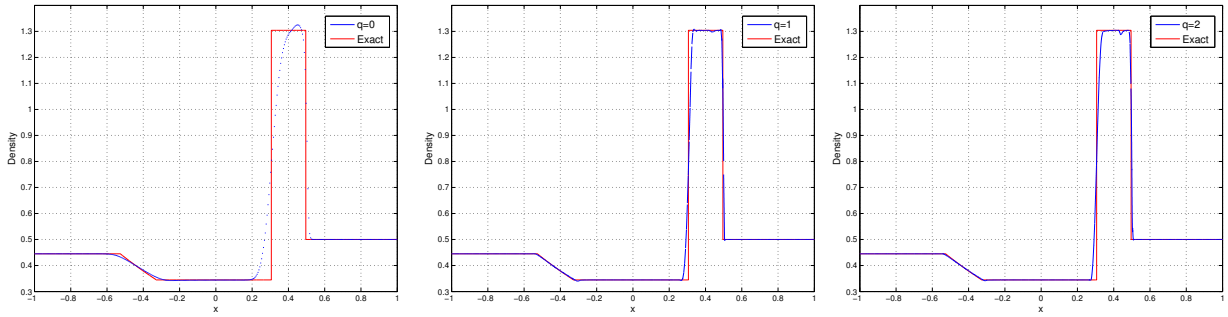

(a) $q = 0$ (b) $q = 1$ (c) $q = 2$

Figure 3: Comparison of the solution of different polynomial order DG versus exact solution, Lax shock tube problem, density is plotted at time $t = 0.2$ on a spatial mesh of 400 elements

.

3. *123 problem*

This problem is designed in Einfeldt et al.[13] to test the performance of a scheme at low densities. It consists of two symmetric strong rarefaction waves and a contact wave of zero speed in the middle. Also this test case can demonstrate the ability of a method to preserve the symmetry. The initial condition of this Riemann problem of the form (36) is set to

$$(\rho_L, u_L, p_L) = (1, -2, 0.4), \qquad (\rho_R, u_R, p_R) = (1, 2, 0.4). \tag{39}$$

We set the final time as $T = 0.15$ and the problem is solved for different DG polynomial order $q = 0, 1, 2$. In general there isn't a control mechanism in our tent pitcher algorithm to keep the mesh symmetric. Since symmetric results are a feature of this test case, the tent pitcher choice criteria were modified to ensure the symmetry of the final mesh for this test case to make the results comparable in terms of their symmetry. The results provided in Figure 4 show the symmetry of the numerical results as well as acceptable handling of the low density contact wave in the middle.

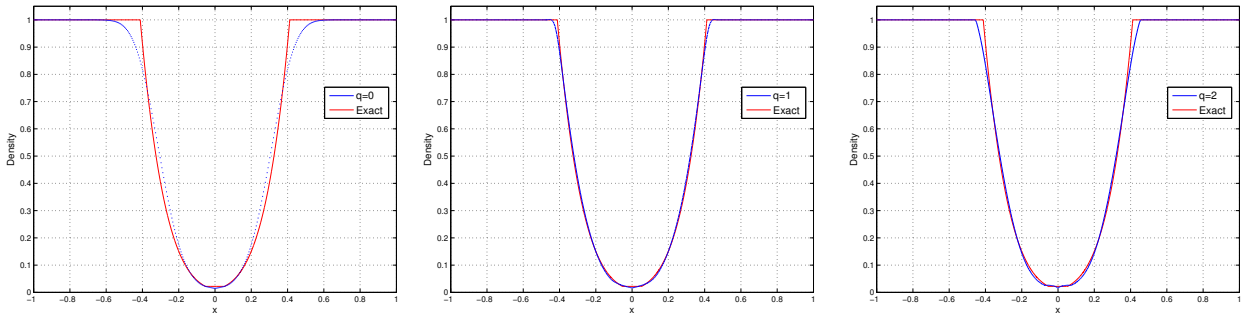

(a) $q = 0$ (b) $q = 1$ (c) $q = 2$

Figure 4: Comparison of the solution of different polynomial order DG versus exact solution, 123 problem, density is plotted at time $t = 0.15$ on a spatial mesh of 400 elements.

4. Shock-entropy wave interaction

This problem was designed by Shu and Osher[33] in order to assess the ability of the scheme to handle the interaction of the shock and sine waves. The initial condition of this Riemann problem of the form (36) is set to

$$(\rho_L, u_L, p_L) = (3.857143, 2.629369, 10.33333), \qquad (\rho_R, u_R, p_R) = (1 + \epsilon sin(25x), 0, 1). \tag{40}$$

When $\epsilon = 0$, the problem is a pure $Ma = 3$ shock moving to the right, otherwise there are some sine waves that interact with this shock. Here ϵ is set to 0.2. Also note that in the original test case[33] the frequency of the wave is $\frac{5}{2\pi}$ while in our settings is increased to $\frac{25}{2\pi}$ for the purpose of scaling down the problem in $x - t$ plane.

The problem is solved for different polynomial order $q = 0, 1, 2$ when the final time is set to $T = 0.36$. The results are provided in Figure 5. Since this problem does not have an exact solution we compare our results with a reference solution obtained using a finite volume scheme developed by Fjordholm[16] with 2000 points. Here we see an acceptable performance of $q = 1, 2$ in resolving the wave interaction structure while $q = 0$ looks more diffusive.

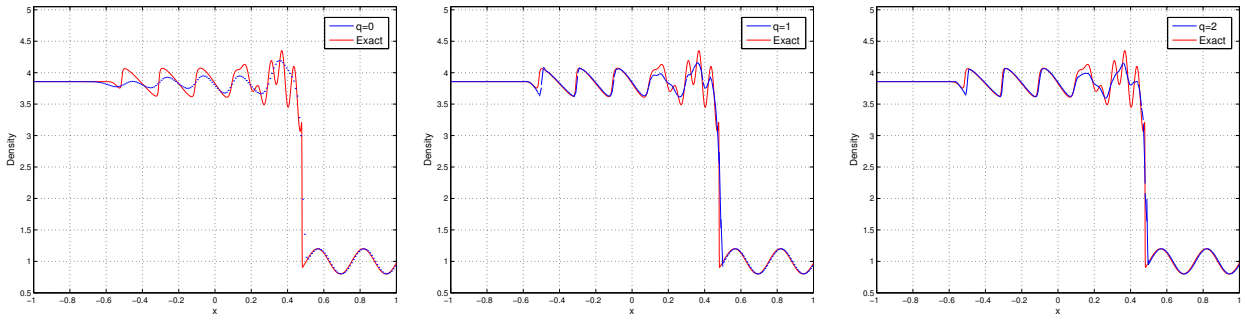

(a) $q = 0$ (b) $q = 1$ (c) $q = 2$

Figure 5: Comparison of the solution of different polynomial order DG versus exact (reference) solution, Shu-Osher shock-entropy wave interaction problem, density is plotted at time $t = 0.36$ on a spatial mesh of 200 elements.

D. Viscosity scaling

Based on the observations in the numerical experiment, results with $q = 2$ usually look more diffusive than with $q = 1$, which might seem somehow counter intuitive. As an explanation for this we looked at the scaling of artificial viscosity proposed by Persson and Peraire.[31] They claim that the viscosity should be chosen as

a function of the resolution accuracy of the approximation space; hence, ε_κ should be scaled of $\mathcal{O}(\frac{h}{q})$ and not just $\mathcal{O}(h)$. Applying this change to (14) yields

$$\varepsilon_\kappa = \frac{(h/q)^\alpha C^{SC} \overline{\mathrm{Res}}_\kappa}{\overline{\nabla \boldsymbol{v}}_\kappa + h^\theta}. \tag{41}$$

We have not redone all of the test cases with the new scaling. Only to give an example of the effect of such a scaling on the diffusive behaviour, we present the comparison of two scaling for Sod and Lax shock tube. Since the scaling (41) reduces to (14) in case $q = 1$ we just present the results for quadratic DG polynomials.

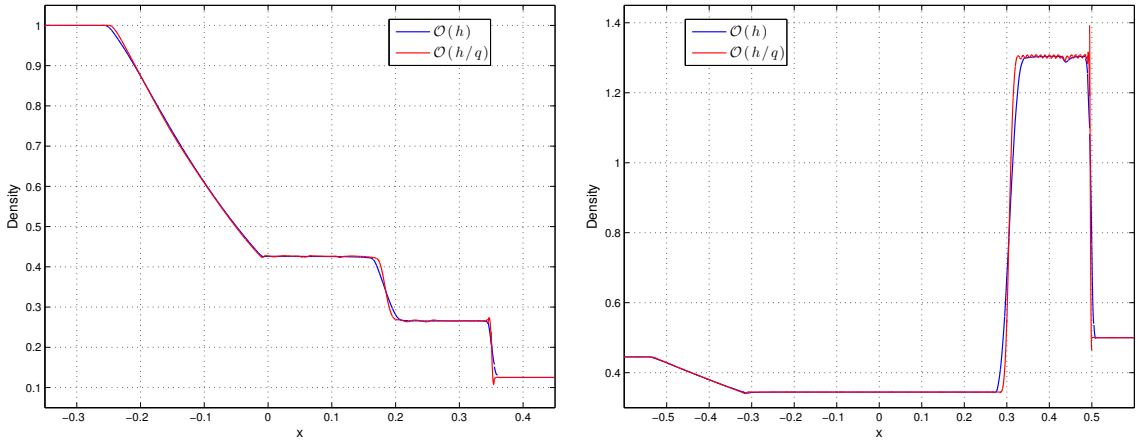

(a) Sod shock tube

(b) Lax shock tube

Figure 6: Comparison of the $\mathcal{O}(h/q)$ scaling proposed in[31] versus $\mathcal{O}(h)$ of[22] on the diffusive behaviour. Sod and Lax shock tube with $q = 2$ and on a spatial domain mesh of 400 elements.

As it is clear from Figure 6, the scaling is considerably effective on the diffusive behaviour of the scheme. As the new scaling makes the shocks much sharper and the solution would be more oscillatory in general and with stronger overshoots. This, or a similar scaling, may be considered for a p convergence study of the scheme proposed in our original publication of the scheme,[42] i.e. as $p \to \infty$ incorporating the p scaling in the convergence analysis to EMV solutions.

V. Conclusion

In this work we presented a high order entropy stable DG scheme in the space-time framework. Our scheme, unlike its predecessors, used residual-based nonlinear shock capturing as the only stabilization mechanism and no streamline diffusion is added to control the residual. Also in order to have computational efficiency we propose to use the tent pitcher algorithm to handle the time marching process.

The timing results look promising compared to the older version of the code which couples all the space-time degrees of freedom at each time slab. In terms of memory usage the tent pitcher method outperforms dramatically due to much fewer degrees of freedom at each level of solution. Considering the fact that the current version of tent pitcher is a preliminary version and not efficient in terms of allocation of the finite element space for each tent, we can expect even better efficiency in future versions. An option to avoid such an excessive allocation cost is to map all elements to a reference element and solve a mapped version of (1) in that element. For more details we refer to the recent work by Gopalakrishnan.[19]

Acknowledgments

The authors are supported by the Deutsche Forschungsgemeinschaft (German Research Association) through grant GSC 111. The first author gratefully acknowledges Joachim Schöberl and Christoph Wintersteiger in TU Wien for the discussion on NetGen/NGSolve and tent pitcher methods during his stay in Vienna in March 2016.

References

[1]R. Abedi, S.-H. Chung, J. Erickson, Y. Fan, M. Garland, D. Guoy, R. Haber, J. M. Sullivan, S. Thite, and Y. Zhou, *Spacetime meshing with adaptive refinement and coarsening*, in Proceedings of the twentieth annual symposium on Computational geometry, ACM, 2004, pp. 300–309.

[2]S. Balay, S. Abhyankar, M. Adams, J. Brown, P. Brune, K. Buschelman, V. Eijkhout, W. Gropp, D. Kaushik, M. Knepley, et al., *Petsc users manual revision 3.5*, tech. rep., Argonne National Laboratory (ANL), 2014.

[3]T. J. Barth, *Numerical methods for gasdynamic systems on unstructured meshes*, in An introduction to recent developments in theory and numerics for conservation laws, Springer, 1999, pp. 195–285.

[4]———, *Simplified discontinuous Galerkin methods for systems of conservation laws with convex extension*, in Discontinuous Galerkin Methods, Springer, 2000, pp. 63–75.

[5]———, *On discontinuous Galerkin approximations of Boltzmann moment systems with Levermore closure*, Computer Methods in Applied Mechanics and Engineering, 195 (2006), pp. 3311–3330.

[6]N. K. Burgess and D. J. Mavriplis, *hp-Adaptive discontinuous Galerkin solver for the Navier-Stokes equations*, AIAA journal, 50 (2012), pp. 2682–2694.

[7]M. H. Carpenter, T. C. Fisher, E. J. Nielsen, and S. H. Frankel, *Entropy stable spectral collocation schemes for the navier-stokes equations: Discontinuous interfaces*, Siam Journal on Scientific Computing, 36 (2014), pp. B835–B867.

[8]M. Ceze and K. J. Fidkowski, *Anisotropic hp-adaptation framework for functional prediction*, AIAA Journal, 51 (2012), pp. 492–509.

[9]P. Chandrashekar, *Discontinuous galerkin method for navier–stokes equations using kinetic flux vector splitting*, Journal of Computational Physics, 233 (2013), pp. 527–551.

[10]B. Cockburn, F. Coquel, and P. LeFloch, *An error estimate for finite volume methods for multidimensional conservation laws*, Mathematics of Computation, 63 (1994), pp. 77–103.

[11]O. Delestre, C. Lucas, P.-A. Ksinant, F. Darboux, C. Laguerre, T.-N.-T. Vo, F. James, and S. Cordier, *Swashes: a compilation of shallow water analytic solutions for hydraulic and environmental studies*, International Journal for Numerical Methods in Fluids, 72 (2013), pp. 269–300.

[12]R. J. DiPerna, *Measure–valued solutions to conservation laws*, Archive for Rational Mechanics and Analysis, 88 (1985), pp. 223–270.

[13]B. Einfeldt, C.-D. Munz, P. L. Roe, and B. Sjögreen, *On godunov-type methods near low densities*, Journal of computational physics, 92 (1991), pp. 273–295.

[14]R. S. Falk and G. R. Richter, *Explicit finite element methods for symmetric hyperbolic equations*, SIAM Journal on Numerical Analysis, 36 (1999), pp. 935–952.

[15]T. C. Fisher and M. H. Carpenter, *High-order entropy stable finite difference schemes for nonlinear conservation laws: Finite domains*, Journal of Computational Physics, 252 (2013), pp. 518–557.

[16]U. S. Fjordholm, *Compac*, 2013. http://folk.ntnu.no/ulriksf/files/compack-1.1B.zip.

[17]———, *High–order accurate entropy stable numerical schemes for hyperbolic conservation laws*, PhD thesis, ETH Zürich, 2013.

[18]U. S. Fjordholm, S. Mishra, and E. Tadmor, *Arbitrarily high–order accurate entropy stable essentially nonoscillatory schemes for systems of conservation laws*, SIAM Journal on Numerical Analysis, 50 (2012), pp. 544–573.

[19]J. Gopalakrishnan, J. Schöberl, and C. Wintersteiger, *Mapped tent pitching schemes for hyperbolic systems*, arXiv preprint arXiv:1604.01081, (2016).

[20]R. Hartmann and P. Houston, *Adaptive discontinuous galerkin finite element methods for the compressible euler equations*, J. Comp. Phys., 183 (2002), pp. 508–532.

[21]R. Hartmann and P. Houston, *Symmetric interior penalty dg methods for the compressible navier–stokes equations i: Method formulation*, Int. J. Num. Anal. Model., 3 (2006), pp. 1–20.

[22]A. Hiltebrand and S. Mishra, *Entropy stable shock capturing space–time discontinuous galerkin schemes for systems of conservation laws*, Numerische Mathematik, 126 (2014), pp. 103–151.

[23]T. J. Hughes and M. Mallet, *A new finite element formulation for computational fluid dynamics: III. the generalized streamline operator for multidimensional advective-diffusive systems*, Computer Methods in Applied Mechanics and Engineering, 58 (1986), pp. 305–328.

[24]F. Ismail and P. L. Roe, *Affordable, entropy-consistent euler flux functions ii: Entropy production at shocks*, Journal of Computational Physics, 228 (2009), pp. 5410–5436.

[25]J. Jaffre, C. Johnson, and A. Szepessy, *Convergence of the discontinuous Galerkin finite element method for hyperbolic conservation laws*, Mathematical Models and Methods in Applied Sciences, 5 (1995), pp. 367–386.

[26]C. Johnson and A. Szepessy, *On the convergence of a finite element method for a nonlinear hyperbolic conservation law*, Mathematics of Computation, 49 (1987), pp. 427–444.

[27]C. Johnson, A. Szepessy, and P. Hansbo, *On the convergence of shock–capturing streamline diffusion finite element methods for hyperbolic conservation laws*, Mathematics of Computation, 54 (1990), pp. 107–129.

[28]S. N. Kružkov, *First order quasilinear equations in several independent variables*, Sbornik: Mathematics, 10 (1970), pp. 217–243.

[29]R. B. Lowrie, P. L. Roe, and B. Van Leer, *Space-time methods for hyperbolic conservation laws*, in Barriers and Challenges in Computational Fluid Dynamics, Springer, 1998, pp. 79–98.

[30]J. Palaniappan, R. B. Haber, and R. L. Jerrard, *A spacetime discontinuous galerkin method for scalar conservation laws*, Computer Methods in Applied Mechanics and Engineering, 193 (2004), pp. 3607–3631.

[31]P.-O. Persson and J. Peraire, *Sub-cell shock capturing for discontinuous galerkin methods*, AIAA paper, 112 (2006), p. 2006.

[32]J. Schöberl, *NETGEN an advancing front 2D/3D-mesh generator based on abstract rules*, Computing and visualization in science, 1 (1997), pp. 41–52.

[33]C.-W. Shu and S. Osher, *Efficient implementation of essentially non-oscillatory shock-capturing schemes*, Journal of Computational Physics, 77 (1988), pp. 439–471.

[34]A. Szepessy, *Convergence of a shock–capturing streamline diffusion finite element method for a scalar conservation law in two space dimensions*, Mathematics of Computation, 53 (1989), pp. 527–545.

[35]———, *Convergence of a streamline diffusion finite element method for a conservation law with boundary conditions*, RAIRO Modelling and Numercial Analysis Modelisations, 25 (1991), pp. 749–783.

[36]E. Tadmor, *The numerical viscosity of entropy stable schemes for systems of conservation laws. I*, Mathematics of Computation, 49 (1987), pp. 91–103.

[37]———, *Entropy stability theory for difference approximations of nonlinear conservation laws and related time–dependent problems*, Acta Numerica, 12 (2003), pp. 451–512.

[38]S. Thite, *Efficient spacetime meshing with nonlocal cone constraints*, arXiv preprint arXiv:0804.0946, (2008).

[39]A. Üngör and A. Sheffer, *Tent-pitcher: A meshing algorithm for space-time discontinuous galerkin methods*, in In proc. 9th intl. meshing roundtable, Citeseer, 2000.

[40]Z. J. Wang, K. Fidkowski, R. Abgrall, F. Bassi, D. Caraeni, A. Cary, H. Deconinck, R. Hartmann, K. Hillewaert, H. T. Huynh, N. Kroll, G. May, P.-O. Persson, B. van Leer, and M. Visbal, *High-order cfd methods: current status and perspective*, International Journal for Numerical Methods in Fluids, 72 (2013), pp. 811–845.

[41]L. Yin, A. Acharya, N. Sobh, R. B. Haber, and D. A. Tortorelli, *A space-time discontinuous galerkin method for elastodynamic analysis*, in Discontinuous Galerkin Methods, Springer, 2000, pp. 459–464.

[42]M. Zakerzadeh and G. May, *On the convergence of a shock capturing discontinuous galerkin method for nonlinear hyperbolic systems of conservation laws*, SIAM Journal on Numerical Analysis, 54 (2016), pp. 874–898.